

# Harmonically trapped Bose-Bose mixtures: a quantum Monte Carlo study

V. Cikojević, L. Vranješ Markić

*Faculty of Science, University of Split, Rudera Boškovića 33, HR-21000 Split, Croatia*

J. Boronat

*Departament de Física, Universitat Politècnica de Catalunya, Campus Nord B4-B5, E-08034 Barcelona, Spain*

(Dated: January 18, 2022)

We study a harmonically confined Bose-Bose mixture using quantum Monte Carlo methods. Our results for the density profiles are systematically compared with mean-field predictions derived through the Gross-Pitaevskii equation in the same conditions. The phase space as a function of the interaction strengths and the relation between masses is quite rich. The miscibility criterion for the homogeneous system applies rather well to the system, with some discrepancies close to the critical line for separation. We observe significant differences between the mean-field results and the Monte Carlo ones, that magnify when the asymmetry between masses increases. In the analyzed interaction regime, we observe universality of our results which extend beyond the applicability regime for the Gross-Pitaevskii equation.

## I. INTRODUCTION

Ultracold Bose-Bose mixtures are currently produced in many laboratories offering the unique possibility of studying the interplay between two Bose-Einstein condensates (BEC) [1–12]. The high tunability of the atomic interactions, thanks to the presence of Feshbach resonances, and the combinations between different elements, different isotopes or different hyperfine levels enrich dramatically the interest in its physical study. Before the advent of BEC gases, the study of Bose-Bose mixtures was purely academic since there was not such a stable system in Nature. Nevertheless, its stability was deeply studied in connection with the stable  $^3\text{He}$ - $^4\text{He}$  mixture at low  $^3\text{He}$  concentration. In particular, it was proved that the Bose-Bose mixtures of isotopic Helium are always unstable and phase separate and that only the right consideration of the Fermi nature of  $^3\text{He}$  atoms could account for its finite miscibility [13–16].

The very low density of the BEC gases makes feasible a theoretical description where atomic interactions are modeled by a single parameter, the  $s$ -wave scattering length. The miscibility of bulk Bose-Bose mixtures can be easily derived within mean-field theory [17–19] and the predictions of this approximation account well for the observed properties in different experiments. However, quite recently this simple argument has been questioned when the mixtures are harmonically trapped and a new parameter, based on the shape of the density profiles, has been suggested [20]. The theoretical descriptions rely on the Gross-Pitaevskii (GP) equation whose range of applicability has been assumed to fit in the relevant experimental setups. Recently, it has been proved that if the interspecies interaction is attractive, instead of repulsive, the mixture can be stable due to the Lee-Huang-Yang correction which cancels the mean-field collapse [21]. This partial cancellation between attractive interspecies and repulsive intraspecies interactions can result in a self-bound (liquid) system, whose existence has been checked theoretically by exact quantum

Monte Carlo calculations [22] and recent experiments with mixtures of ultracold  $^{39}\text{K}$  atoms in different internal states [23, 24].

In the present paper, we report results of harmonically trapped repulsive Bose-Bose mixtures in different interaction regimes and with different masses for the constituents. Our approach is microscopic and relies on the use of quantum Monte Carlo methods able to solve exactly a given many-body Hamiltonian for Bose systems (within some statistical noise). The number of particles of our system is much smaller than the typical values used in GP calculations due to the complexity of our approach but this allows for an accurate study of effects going beyond the mean-field treatment. The numerical simulations have been carried out for different combinations of the interaction strengths, covering the mixed and phase separated regimes. In agreement with previous GP results, the miscibility rule derived for homogeneous gases fails to describe some of the results.

The rest of the paper is organized as follows. In the next Section we introduce the theoretical method used for the study. Sec. III contains the density profiles corresponding to the points of the phase diagram here analyzed, both in miscible and phase-separated regimes. In Sec. IV, we study the scaling in terms of the GP interaction strength. Sec. V discusses the universality of our results by changing the model potential. Finally, Sec. VI reports the main conclusions of our work.

## II. METHODS

We study a mixture of two kind of bosons with masses  $m_1$  and  $m_2$ , harmonically confined and at zero tempera-

ture. The Hamiltonian of the system is

$$H = -\frac{\hbar^2}{2} \sum_{\alpha=1}^2 \sum_{i=1}^{N_{\alpha}} \frac{\nabla_i^2}{m_{\alpha}} + \frac{1}{2} \sum_{\alpha,\beta=1}^2 \sum_{i_{\alpha},j_{\beta}=1}^{N_{\alpha},N_{\beta}} V^{(\alpha,\beta)}(r_{i_{\alpha}j_{\beta}}) + \sum_{\alpha=1}^2 \sum_i^N V_{\text{ext}}^{(\alpha)}(\mathbf{r}_i). \quad (1)$$

The mixture is composed of  $N = N_1 + N_2$  particles, with  $N_1$  and  $N_2$  bosons of type 1 and 2, respectively. The interaction between particles is modeled by the potentials  $V^{(\alpha,\beta)}(r_{i_{\alpha}j_{\beta}})$  and the confining potential is a standard harmonic term, with frequencies that can be different for each species,

$$V_{\text{ext}}^{(\alpha)}(\mathbf{r}) = \frac{1}{2} m_{\alpha} \omega_{\alpha}^2 r^2. \quad (2)$$

The many-body problem is solved by means of the diffusion Monte Carlo method (DMC), a nowadays standard tool for the ab initio study of quantum fluids and solids. DMC solves stochastically the imaginary-time  $N$ -body Schrödinger equation in an exact way for bosons within some statistical noise [25]. In a natural way, DMC recovers the mean-field results when the system is dilute enough and can go much beyond since no perturbative approximations are assumed. In brief, DMC turns the Schrödinger equation into a diffusion process in imaginary time with a branching term that replicates the energetically favorable configurations and eliminates the rest. In order to reduce the variance in the statistical averages it is usual to introduce importance sampling through a trial wave function, that drives the random walk away from singularities and focuses the sampling where one reasonable expects that the ground-state wave function is large. In the present problem, we have chosen a Jastrow model for the trial wave function,

$$\Psi(\mathbf{R}) = \prod_{1=i<j}^{N_1} f^{(1,1)}(r_{ij}) \prod_{1=i<j}^{N_2} f^{(2,2)}(r_{ij}) \prod_{i,j=1}^{N_1,N_2} f^{(1,2)}(r_{ij}) \times \prod_{i=1}^{N_1} h^{(1)}(r_i) \prod_{i=1}^{N_2} h^{(2)}(r_i), \quad (3)$$

with  $\mathbf{R} = \{\mathbf{r}_1, \dots, \mathbf{r}_N\}$ ,  $f^{(\alpha,\beta)}(r)$  the two-body Jastrow factors accounting for the pair interactions between  $\alpha$  and  $\beta$  type of atoms, and  $h^{(\alpha)}(r)$  the one-body terms related to the external harmonic potential.

As one of the objectives of our work is to estimate the validity regime for a mean-field approach we have also studied the problem by solving the Gross-Pitaevskii (GP) equations. In this case, one assumes contact interactions between particles,

$$V^{(\alpha,\beta)}(r_{i_{\alpha}j_{\beta}}) = g_{\alpha\beta} \delta(|\mathbf{r}_{i_{\alpha}} - \mathbf{r}_{j_{\beta}}|), \quad (4)$$

with strengths

$$g_{\alpha,\beta} = \frac{2\pi\hbar^2 a_{\alpha\beta}}{\mu_{\alpha\beta}}, \quad (5)$$

with  $\mu_{\alpha\beta}^{-1} = m_{\alpha}^{-1} + m_{\beta}^{-1}$  the reduced mass and  $a_{\alpha\beta}$  the  $s$ -wave scattering length of the two-body interaction between  $\alpha$  and  $\beta$  particles.

With the Hartree-Fock *ansatz*,

$$\Psi(\mathbf{R}) = \prod_{i=1}^{N_1} \phi_1(\mathbf{r}_i, t) \prod_{j=1}^{N_2} \phi_2(\mathbf{r}_j, t) \quad (6)$$

one obtains the coupled GP equations for the mixture [17],

$$i\hbar \frac{\partial \phi_1(\mathbf{r}, t)}{\partial t} = \left( -\frac{\hbar^2}{2m_1} \nabla^2 + V_{\text{ext}}^{(1)}(\mathbf{r}) + g_{11} |\phi_1(\mathbf{r}, t)|^2 + g_{12} |\phi_2(\mathbf{r}, t)|^2 \right) \phi_1(\mathbf{r}, t), \quad (7)$$

$$i\hbar \frac{\partial \phi_2(\mathbf{r}, t)}{\partial t} = \left( -\frac{\hbar^2}{2m_2} \nabla^2 + V_{\text{ext}}^{(2)}(\mathbf{r}) + g_{22} |\phi_2(\mathbf{r}, t)|^2 + g_{12} |\phi_1(\mathbf{r}, t)|^2 \right) \phi_2(\mathbf{r}, t). \quad (8)$$

We have solved the GP equations (7,8) by imaginary-time propagation using a 4th order Runge-Kutta method.

### III. PHASE SPACE

We have explored the phase space of the Bose-Bose mixture using the DMC method and, in all cases, we have compared DMC with GP results in the same conditions. We drive our attention to the density profiles of both species since our main goal is to determine if the systems are miscible or phase separated. The results contained in this Section have been obtained by using hard-core potentials between the different particles,

$$V^{(\alpha\beta)}(r) = \begin{cases} \infty, & r \leq a_{\alpha\beta} \\ 0, & r > a_{\alpha\beta} \end{cases}, \quad (9)$$

with  $a_{\alpha\beta}$  the radius of the hard sphere which coincides with its  $s$ -wave scattering length. The Jastrow factor in the trial wave function (3) is chosen as the two-body scattering solution,  $f^{(\alpha,\beta)}(r) = 1 - a_{\alpha\beta}/r$ , and the one-body term corresponds to the exact single-particle ground-state wave function,  $h^{(\alpha)}(r) = \exp(-r^2/(2a_{\alpha}^2))$ . The length  $a_{\alpha}$  is optimized variationally but, even for the strongest interaction regime here studied, its value is at most 10% larger than the one of the non-interacting system,  $l_{\text{ho},\alpha} = \sqrt{\hbar/(m_{\alpha}\omega_{\alpha})}$ . The one-body terms  $h^{(\alpha)}(r)$  confine the particles to move within a finite volume and thus open boundary conditions are used. The influence of internal parameters of the DMC calculations, such as the number of walkers and the imaginary-time step, is analyzed and the reported results are converged with respect to them. The density profiles that we report are derived using the mixed estimation since we have checked that

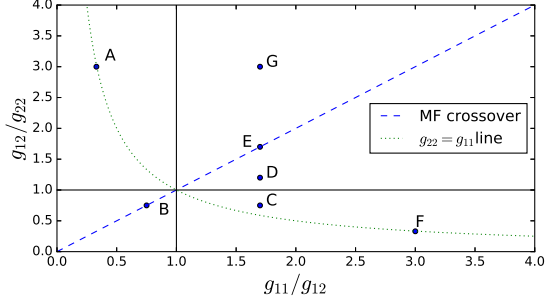


FIG. 1. Representation of the phase space for the mixture as a function of the interaction strengths  $g_{\alpha\beta}$ . The points correspond to the cases studied, with coordinates given in Table I. The mean-field theory for homogeneous system predicts separation (mixing) for all the points above (below) the mean-field critical line (dashed line). The dotted (green) line stands for points where  $g_{11} = g_{22}$ .

Label	$g_{12}/g_{22}$	$g_{11}/g_{12}$	$\Delta$
A	3.0	0.33	-0.89
B	0.75	0.75	0
C	0.75	1.7	1.27
D	1.2	1.7	0.42
E	1.7	1.7	0
F	0.33	3	8
G	3	1.7	-0.43

TABLE I. Representative phase space points analyzed in our study. The values of  $\Delta$  are obtained from Eq. (10).

the correction introduced by using pure estimators [26] is at the same level as the typical statistical noise.

As in Ref. [20], we plot the phase space in terms of the adimensional variables  $g_{12}/g_{22}$  and  $g_{11}/g_{12}$ . In Fig. 1 we plot it showing the different regimes, with the line  $g_{12}^2 = g_{11}g_{22}$  standing for the critical line separating miscibility and phase separation, using the mean-field criterion. In the figure, we plot the points which we have studied; they are selected to cover the most interesting areas of the phase space. In Table I, we report the specific coordinates of the interaction strengths.

As usual in the study of Bose-Bose mixtures we define an adimensional parameter  $\Delta$ ,

$$\Delta = \frac{g_{11}g_{22}}{g_{12}^2} - 1, \quad (10)$$

which classifies the regimes of phase separation ( $\Delta < 0$ ) and miscibility ( $\Delta > 0$ ) according to the mean-field treatment of bulk mixtures. When  $\Delta = 0$  we are on the critical line separating both regimes (dashed line in Fig. 1). In the results reported below, we also calculate the parameter  $\Delta n$  defined as [20]

$$\Delta n = \frac{\rho_1(0)}{\max \rho_1(r)} - \frac{\rho_2(0)}{\max \rho_2(r)}, \quad (11)$$

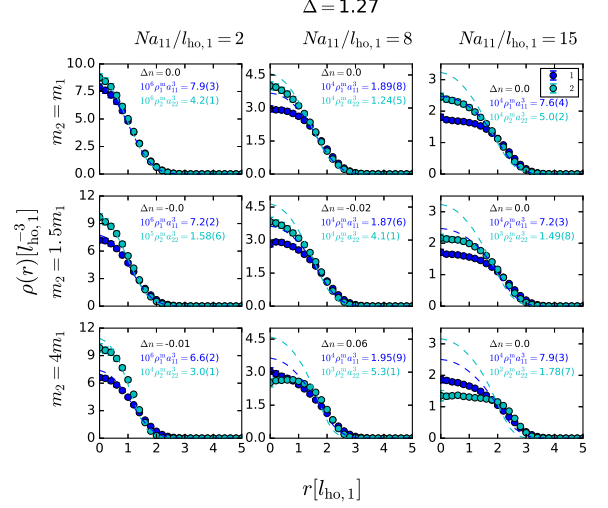


FIG. 2. Point C of the phase space. The points correspond to the DMC results and the lines to the solution of the GP equations for the same system. For each case we report the gas parameter of each species calculated at the maximum of the density profile.

which compares the value of the density profiles  $\rho_\alpha(r)$  at the origin  $r = 0$  with its maximum value. Then,  $\Delta n \simeq 0$  when the peaks of both density profiles coincide to be at the origin (mixed state) or when the ratio of the central and maximum density is the same for both species, which occurs when two species of the same mass separate to two blobs. For other types of phase separation  $|\Delta n| > 0$ .

The density profiles reported in this Section have been obtained with a total number of particles  $N = 200$  and considering a balanced mixture, i.e.,  $N_1 = N_2$ . We have repeated some calculations considering  $N_1/N_2 = \sqrt{g_{22}/g_{11}}$ , which is the optimal balance from the mean-field theory [21], and the differences in energy with respect to  $N_1 = N_2$  are at most 10%. Therefore, we concentrate on the balanced mixture. The role of the confining frequencies  $\omega_\alpha$  is a bit more relevant since we have observed changes in the results that can reach the 30%. In general, the energies are lower when the frequencies obey the rule  $m_1\omega_1^2 = m_2\omega_2^2$  which corresponds to applying the same harmonic confinement for both species. Therefore, the results presented below correspond always to this choice.

### A. $\Delta > 0$

When  $\Delta > 0$  the mean-field criterion predicts mixing between the two species. We have explored the confined system in three different points of the phase space. We start with point C, with  $\Delta = 1.27$  and the  $g_{\alpha\beta}$  values reported in Table I. In Fig. 2, we show the density profiles of both species. In all cases, we use as unit length the harmonic oscillator length  $l_{ho,1}$  of species 1. In the nine

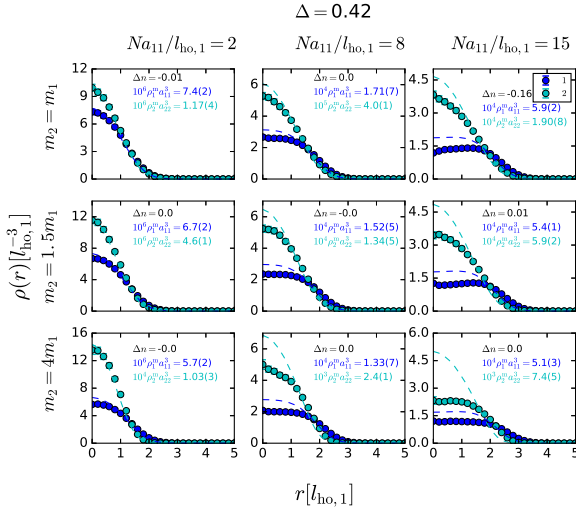


FIG. 3. Point D of the phase space. The points correspond to the DMC results and the lines to the solution of the GP equations for the same system.

subfigures of Fig. 2, going from left to right we increase the parameter  $Na_{11}/l_{ho,1}$ , and from top to bottom we increase the mass of species 2. The parameter  $Na_{11}/l_{ho,1}$  is chosen because it is the mean-field scaling variable contained in the GP equation. As we keep the total number of particles  $N$  fixed, increasing that parameter means to increase the scattering length of the 11 interaction and thus making  $g_{11}$  larger. As the coordinates in the phase space are fixed at the point C, increasing  $g_{11}$  implies that also the other strengths  $g_{12}$  and  $g_{22}$  increase. Therefore, moving to the right in the panels of Fig. 2 means an increase of both the interspecies and intraspecies interaction. Moving down in the panels, for a fixed value  $Na_{11}/l_{ho,1}$ , means an increase of the mass of species 2 and therefore an increase of the scattering lengths  $a_{12}$  and  $a_{22}$  because the couplings  $g_{12}$  and  $g_{22}$  are kept constant.

The density profiles shown in Fig. 2 show in all cases a mixed state, with  $\Delta n \simeq 0$  (11). In the leftmost column, when the interaction is very soft, we appreciate that  $\rho^{(\alpha)}(r)$  are basically Gaussians, following the shape of the non-interacting gas. When  $m_2$  grows, they are still Gaussians but slightly different in shape because the frequencies are different. The Gaussian profiles disappear progressively moving to the right due to the increase of interactions. The comparison between DMC and GP shows agreement when the interaction is low and they clearly depart when  $Na_{11}/l_{ho,1}^{(1)}$  grows. The DMC profiles show the emergence of a plateau close to  $r = 0$ , in significant contrast with the GP prediction. The departure of DMC and GP becomes larger when the gas parameter (included in each panel in Fig. 2, calculated near the maximum of each density profile), grows.

Density profiles for points D ( $\Delta = 0.42$ ) and F ( $\Delta = 8$ ) are reported in Figs. 3 and 4, respectively. The results

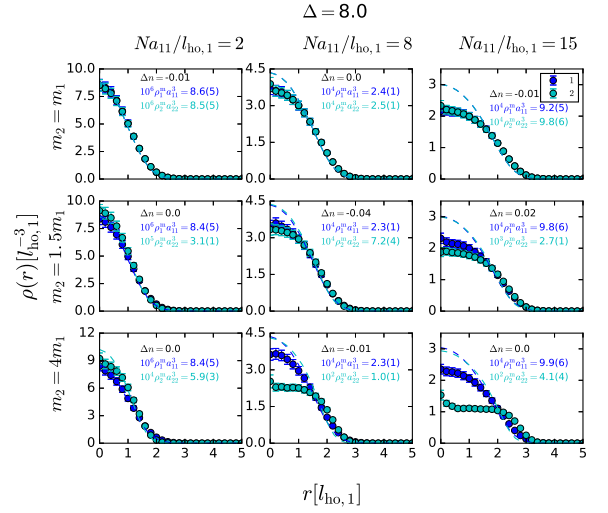


FIG. 4. Point F of the phase space. The points correspond to the DMC results and the lines to the solution of the GP equations for the same system.

are qualitatively similar to the ones of point C, showing mixing in both cases. Point F is deeply located in the mixed part of the phase space (large  $\Delta$  value) and the agreement with GP is, in this case, quite satisfactory except quantitatively when the mass difference is large and the strength of the interaction increases. Point D, with a small  $\Delta$  value, shows slightly more significant departures from GP predictions that again increase when the difference in mass between both species increases.

## B. $\Delta = 0$

We have studied two points (B and E, see Table I) of the phase space which are illustrative of the  $\Delta = 0$  case. Assuming mean-field theory, this corresponds to the critical line for mixing in bulk mixtures.

In point B, we have  $g_{12}/g_{22} = 0.75$  and  $g_{11}/g_{12} = 0.75$ . With these values,  $g_{22} > g_{12} > g_{11}$ , and thus one expects that species 2 goes out of the trap center because it is more repulsive than species 1. This effect is emphasized when  $m_2 > m_1$  because the relation between scattering lengths has an additional factor  $m_2/m_1$ . In Fig. 5, we can see the evolution of the density profiles as a function of the interaction strength and mass ratio. When the system is only weakly interacting (left column) one appreciates Gaussian profiles that coincide with GP predictions. The situation changes when the interaction grows (second and third columns) as we can see that the two systems start to phase separate, a feature that is measured by the positive value of the factor  $\Delta n$  (11). If the difference in mass is enlarged, bottom panels, one can see that the phase separation is even more clear. In this case, the heaviest component (2) is manifestly going out of the center and thus it surrounds the core, mainly occupied



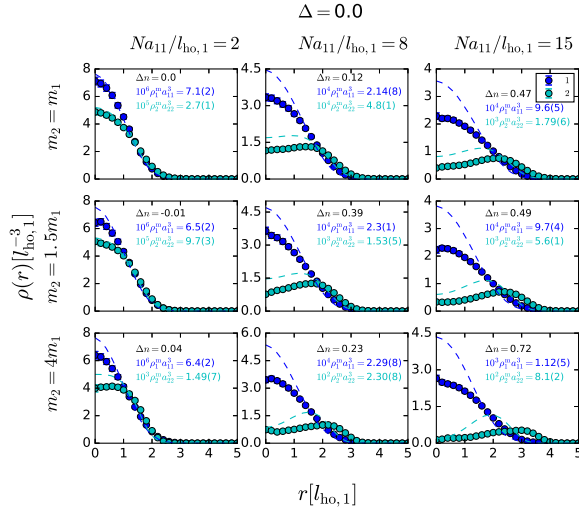


FIG. 5. Point B of the phase space. The points correspond to the DMC results and the lines to the solution of the GP equations for the same system.

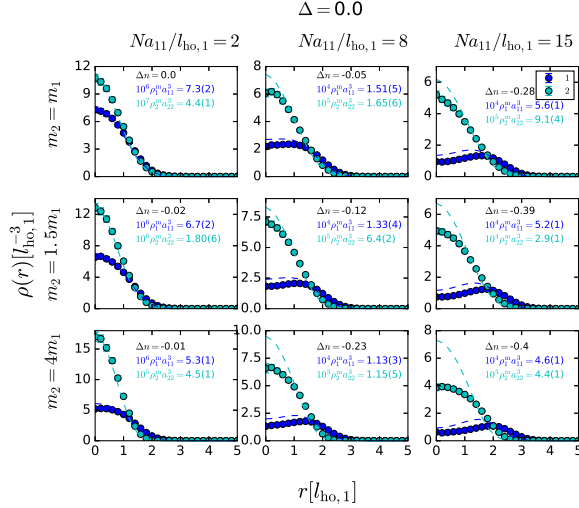


FIG. 6. Point E of the phase space. The points correspond to the DMC results and the lines to the solution of the GP equations for the same system.

by the species 1. Comparison with GP shows that there is a qualitative agreement with DMC but quantitatively GP is rather inaccurate, specially when the mass ratio is  $m_2/m_1 = 4$ .

In point E, we are still in the critical line  $\Delta = 0$  but now the relation of interaction strengths is inverted with respect to point B. That is,  $g_{22} < g_{12} < g_{11}$ . Therefore, one now expects species 2 occupying the center and species 1 moving to the external part of the trap. This is reflected in the negative values of the parameter  $\Delta n$  which are reported for every panel in Fig. 6. The increase of the factor  $m_2/m_1$  goes in reverse direction and slightly compensates the increase in  $a_{22}$ . However, it is

shown not to be large enough to change the description. Comparing with Fig. 5, the phase separation is not complete because one can see that there is always a finite fraction of species 1 close to the center.

### C. $\Delta < 0$

In this subsection, we move to points of the phase space where phase separation is expected. We have studied two representative points of the phase space, points A and G (see Table I).

In point A,  $g_{12}/g_{22} = 3$  and  $g_{11}/g_{12} = 1/3$  producing  $\Delta = -0.89$ . The relation of strengths is now  $g_{11} = g_{22} < g_{12}$ . By going from left to right in the panels of Fig. 7 one can see that the mixture phase separates when the interaction between atoms is more important than the one-body confining harmonic potential. When the masses of both species are equal, one identifies a phase separation in form of two symmetric separated blobs [18, 19], similar to what one would observe in a bulk system. This is also consistent with  $\Delta n = 0$ . Again, the mean-field prediction becomes quantitatively worse, as the interaction strength and the difference in mass between the two components increase. However, although it is not visible from the radial profiles, in all cases of point A there is at least partial phase separation in two blobs. In order to show this, we have calculated the  $P(z, \rho)$  distribution, where the  $z$ -direction is defined as a line passing through the two centers of mass, with the second component being in the positive  $z$ -direction.  $z = 0$  is the geometric center between the two centers of mass. The second variable,  $\rho$ , is just the distance of a single particle from this line. Results are normalized such that  $\int 2\pi\rho d\rho dz P(z, \rho) = N/2$ . The results in the two illustrative cases are presented in Fig. 8 and 9. In the case of equal masses and  $Na_{11}/l_{ho,1} = 2$  (Fig. 8) although both species overlap significantly, the maxima of their probability distributions are clearly separated. In fact the average distance of their centers of mass is about  $0.4l_{ho,1}$ . Increasing  $Na_{11}/l_{ho,1}$  the overlap between the two species decreases and a clear two-blob structure becomes visible, with the average distance between the two centers of mass becoming  $3l_{ho,1}$ . The increase of the mass difference of the two species also favors their separation. The extreme case of  $m_2 = 4m_1$  and  $Na_{11}/l_{ho,1} = 15$  is shown in Fig. 9. We observe that the two species are clearly separated in two blobs and more spread in both the  $\rho$  and  $z$  directions than in Fig. 8, due to the larger repulsive interspecies interaction. DMC predicts the more massive component to be closer to the center of the trap, unlike GP.  $|\Delta n| > 0$  is quite large, but remarkably has opposite sign in GP and DMC.

In the last point (G), one expects phase separation because  $\Delta = -0.43$ . The relation of strengths is now  $g_{11} > g_{12} > g_{22}$ . We clearly observe a phase separated system for medium and large interactions and a mixed one when  $Na_{11}/l_{ho,1} = 2$ . The lighter particle moves

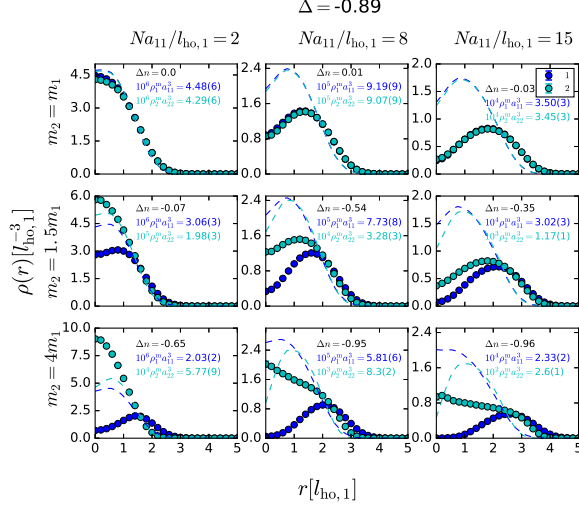


FIG. 7. Point A of the phase space. The points correspond to the DMC results and the lines to the solution of the GP equations for the same system.

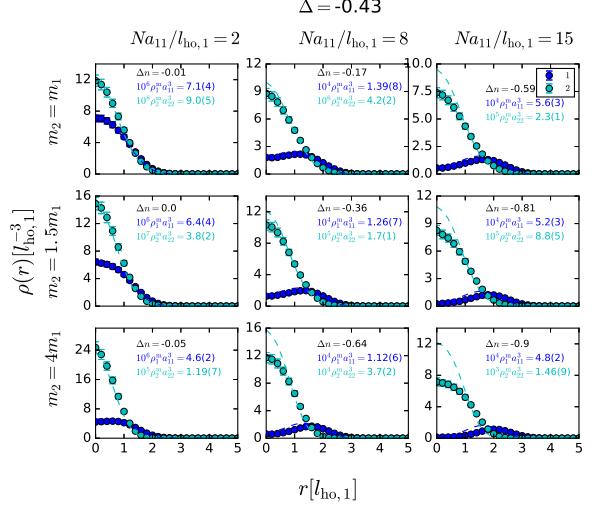


FIG. 10. Point G of the phase space. The points correspond to the DMC results and the lines to the solution of the GP equations for the same system.

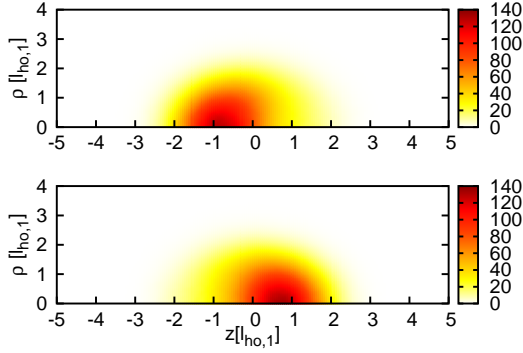


FIG. 8. Point A of the phase space for  $m_1 = m_2$  and  $Na_{11}/l_{ho,1} = 2$ .  $z$ -axis corresponds to the line going through the centers of mass of the two components, while  $\rho$  corresponds to the distance of a particle from that line. Top and bottom panels stand for the distribution of species 1 and 2, respectively.

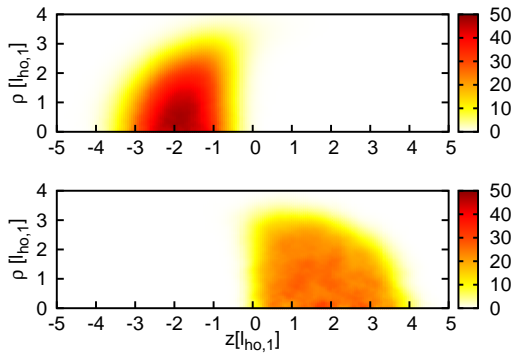


FIG. 9. Same as Fig. 8 (point A) for  $m_2 = 4m_1$  and  $Na_{11}/l_{ho,1} = 15$ .

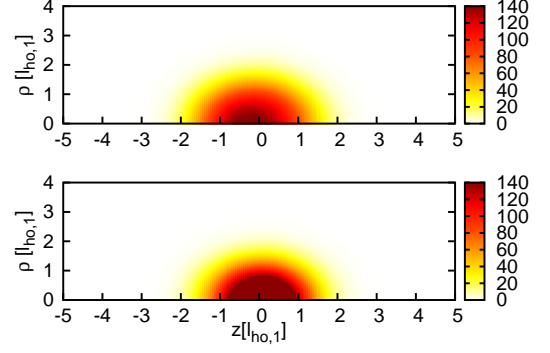


FIG. 11. Same as Fig. 8 (point G) for  $m_2 = m_1$  and  $Na_{11}/l_{ho,1} = 2$ .

progressively out of the center and finally, when the relation of masses is large, it surrounds completely the heavier one, which occupies the center of the trap. Contrarily to point A, here the GP description is in nice agreement with the DMC data even when the difference in masses is large. To get a better visualization of this point G, we show in Figs. 11 and 12 the function  $P(z, \rho)$  defined above in the same conditions as in Figs. 8 and 9. We can see that Fig. 11 shows a mixed configuration whereas Fig. 12 reports a two ring structure, in agreement with what is observed in the density profiles of this point (Fig. 10).

#### IV. SCALING WITH THE INTERACTION PARAMETER $Na_{11}/l_{ho,1}$

In the previous Section, we have plotted the density profiles considering the parameter  $Na_{11}/l_{ho,1}$  as a scal-

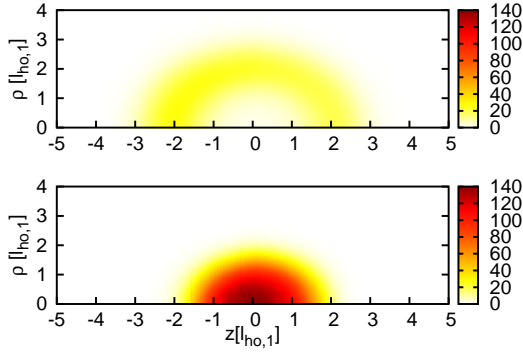


FIG. 12. Same as Fig. 8 (point G) for  $m_2 = 4m_1$  and  $Na_{11}/l_{ho,1} = 15$ .

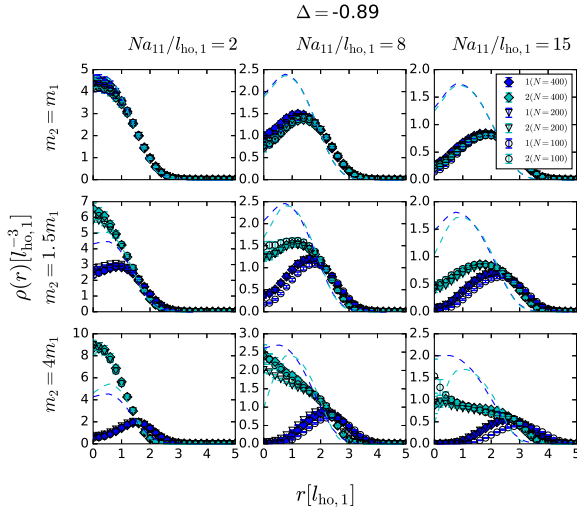


FIG. 13. Scaling on the GP parameter in point A of the phase space. Different points correspond to different number of particles  $N$ .

ing parameter to determine the strength of the interactions. For a given value of this adimensional parameter we have then changed the relation of masses between the two species. This parameter has been taken from the GP equation for a single Bose gas harmonically confined where it is proved to be the *only* input parameter of the calculations. In this section, we check if this is also true in the case of mixtures, both in regimes where DMC results and GP ones essentially coincide and in others where we have observed significant discrepancies.

We have chosen two illustrative cases of both situations. In particular, points A and E of the phase space (see Table I). In both cases we have changed independently  $N$  and  $a_{11}$  in such a way to keep the GP parameter as equal. To this end, we have used a system with  $N = 100 + 100$  and a smaller one, composed by half the number of particles  $N = 50 + 50$ .

In Fig. 13, we report the results of this analysis for point A. The results of the density profiles are all nor-

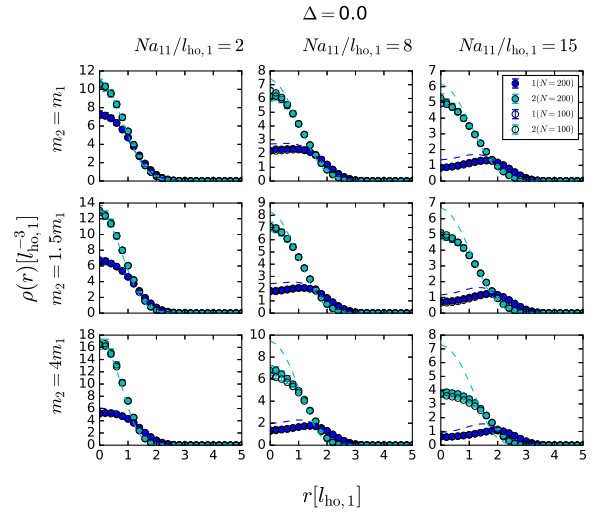


FIG. 14. Scaling on the GP parameter in point E of the phase space. Solid and open points stand for results with  $N = 200$  and  $N = 100$ , respectively.

malized to sum up to 200 in order to make the comparison easier. As we commented in the previous Section, point A is the one where we have observed the largest departures from the GP results. The figures shows excellent agreement when the interaction is low and some discrepancies when the GP parameter grows. However, the effect is not dramatic and affects only the heaviest species. It is remarkable that even in situations like the ones of Fig. 13, where GP strongly departs from DMC, one can still observe a very reasonable scaling with the GP interaction parameter. Moreover, we can see that our results converge for a number of particles  $N \geq 200$  and that these converged results still show discrepancies with the GP density profiles.

Point E was one of the points where the agreement between GP and DMC was better. In Fig. 14, we study the dependence of the density profile results on the GP parameter as a scaling factor. In this case, the agreement is practically perfect because the discrepancies are just of the order of the error bars.

## V. UNIVERSALITY TEST

A relevant point in our numerical simulations is the influence of the model potential on the results. Universality in these terms means that the interaction can be fully described by a single parameter, the  $s$ -wave scattering length, as it corresponds to a very dilute system. In all the previous results we have used a hard-core model for the interactions between the atoms (9). In this Section, we compare these results with other ones obtained with a 10-6 potential,

$$V^{(\alpha\beta)}(r) = \frac{\hbar^2}{2\mu_{\alpha\beta}} V_0 \left[ \left( \frac{r_0}{r} \right)^{10} - \left( \frac{r_0}{r} \right)^6 \right], \quad (12)$$

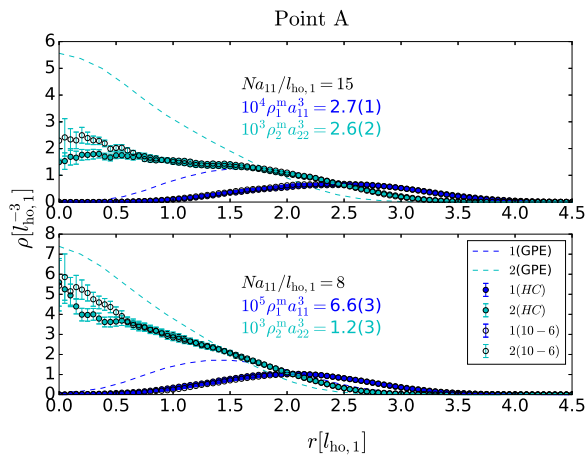


FIG. 15. DMC results for two models are compared to GP results for two values of GP parameter in point A .

whose  $s$ -wave scattering length is analytically known [27]. We fix the parameter  $r_0 = 2a_{\alpha\beta}$  for all cases and modify the strength  $V_0$  to reproduce the desired scattering length. In Eq. (12), the parameter  $\mu_{\alpha\beta}$  is the reduced mass,  $\mu_{\alpha\beta} = m_{\alpha}m_{\beta}/(m_{\alpha} + m_{\beta})$ .

Our analysis has been performed for  $m_2 = 1.5m_1$ ,  $N = 100 + 100$  particles, and considering equal harmonic frequencies  $\omega_1 = \omega_2$ . Two interaction strengths have been used,  $Na_{11}/l_{ho,1} = 8$  and 15. As in the previous Section, we have studied points E and A of the phase space, i.e., those characteristic of agreement and disagreement with GP.

In Fig. 15, we show the density profiles of point A, obtained using the two model potentials normalized in the same way. We can see an overall agreement between both results with only some differences in the estimation of the density in the center. Close to  $r = 0$  the statistical fluctuations are bigger due to the normalization in a small volume. This feature is always present but we observe that these fluctuations are larger in the case of the 10-6 potential (12).

In Fig. 16, we analyzed the same for point E in which we are closer to an effective mean-field description. The comparison also shows a good agreement between results obtained for both potentials, with some differences in the inner core of the trap.

We have verified in other points of the phase space the universality of our results and the conclusion is that this is maintained with respect to the character of the system (miscible or phase separated) and also the overall shape of the density profiles. The influence of the model potential is at the scale of our statistical fluctuations, except close to  $r = 0$  where small differences are observed in some cases.

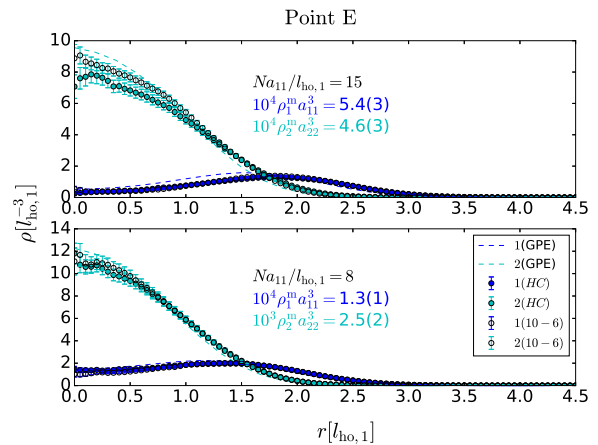


FIG. 16. DMC results for two models are compared to GP results for two values of GP parameter in point E.

## VI. DISCUSSION

Using the diffusion Monte Carlo method, able to provide exact results for bosonic systems, we have explored the phase space of an harmonically confined Bose-Bose mixture at zero temperature. Our results are compared in all cases with a mean-field Gross-Pitaevskii calculation in the same conditions. As expected, our DMC results agree better with the GP ones when the strength of interactions is small and worsens progressively when that grows. In spite of the fact that the prediction for miscibility or phase separation is coincident in both cases, it is also true that the density profiles can be rather different. The relevance of quantum fluctuations, which makes the density profiles to depart from the GP ones, depends on the dimensionality of the system. It is well known [28, 29] that they become much more significant in the case of one dimension, since the Lee-Huang-Yang term scales as  $n^{1/2}$  instead of the three-dimensional law  $n^{3/2}$ .

Our results are by construction exact and go beyond mean-field, showing the limits of this approach. A systematic trend in which GP fails is the dependence on the mass of the two species. When the asymmetry in the masses grows GP becomes clearly wrong in some cases. That could be argued to be an effect of the interaction model used in DMC but our results contradict this point, within the range of interactions here explored.

The tunability of atomic interactions and the possibility of using atoms with different mass ratios makes this system specially rich. The phase space shows regimes of miscibility and, interestingly, two different situations for phase separation, two blobs or in-out spherical separation, depending in the relation of masses and interaction strength. It would be very interesting to produce in the lab smaller systems, with hundreds of atoms, to check the departure of the physics from the mean-field GP treatment. In this way, one can start to enter into the realm of fully quantum many-body physics.



## ACKNOWLEDGMENTS

This work has been supported in part by the Croatian Science Foundation under the project number IP-2014-

09-2452 and MINECO (Spain) Grants No. FIS2014-56257-C2-1-P and No. FIS2017-84114-C2-1-P. The computational resources of the Isabella cluster at Zagreb University Computing Center (Srce) and Croatian National Grid Infrastructure (CRO NGI) were used.

- 
- [1] D. S. Hall, M. R. Matthews, J. R. Ensher, C. E. Wieman, and E. A. Cornell, *Phys. Rev. Lett.* **81**, 1539 (1998).
  - [2] P. Maddaloni, M. Modugno, C. Fort, F. Minardi, and M. Inguscio, *Phys. Rev. Lett.* **85**, 2413 (2000).
  - [3] S. B. Papp, J. M. Pino, and C. E. Wieman, *Phys. Rev. Lett.* **101**, 040402 (2008).
  - [4] G. Thalhammer, G. Barontini, L. De Sarlo, J. Catani, F. Minardi, and M. Inguscio, *Phys. Rev. Lett.* **100**, 210402 (2008).
  - [5] S. Sugawa, R. Yamazaki, S. Taie, and Y. Takahashi, *Phys. Rev. A* **84**, 011610 (2011).
  - [6] D. J. McCarron, H. W. Cho, D. L. Jenkin, M. P. KÄp-pinger, and S. L. Cornish, *Phys. Rev. A* **84**, 011603 (2011).
  - [7] A. Pasquiou, A. Bayerle, S. M. Tzanova, S. Stellmer, J. Szczepkowski, M. Parigger, R. Grimm, and F. Schreck, *Phys. Rev. A* **88**, 023601 (2013).
  - [8] I. Ferrier-Barbut, M. Delahaye, S. Laurent, A. T. Grier, M. Pierce, B. S. Rem, F. Chevy, and C. Salomon, *Science* **345**, 1035 (2014).
  - [9] L. Wacker, N. B. Jorgensen, D. Birkmose, R. Horchani, W. Ertmer, C. Klempt, N. Winter, J. Sherson, and J. J. Arlt, *Phys. Rev. A* **92**, 053602 (2015).
  - [10] T. Bienaim  , E. Fava, G. Colzi, C. Mordini, S. Serafini, C. Qu, S. Stringari, G. Lamporesi, and G. Ferrari, *Phys. Rev. A* **94**, 063652 (2016).
  - [11] R. N. Bisset, P. G. Kevrekidis, and C. Ticknor, *Phys. Rev. A* **97**, 023602 (2018).
  - [12] T. A. Schulze, T. Hartmann, K. K. Voges, M. W. Gempel, E. Tiemann, A. Zenesini, and S. Ospelkaus, *Phys. Rev. A* **97**, 023623 (2018).
  - [13] W. E. Massey, C-W Woo, and H-T Tan, *Phys. Rev. A* **1** 519 (1970).
  - [14] M. D. Miller, *Phys. Rev. B* **18**, 4730 (1978).
  - [15] K. E. K  rten and C. E. Campbell, *Phys. Rev. B* **26**, 124 (1982).
  - [16] T. Chakraborty, *Phys. Rev. B* **26**, 6131 (1982).
  - [17] T-L. Ho and V. B. Shenoy, *Phys. Rev. Lett.* **77**, 3276 (1996).
  - [18] H. Pu and N. P. Bigelow, *Phys. Rev. Lett.* **80**, 1130 (1998).
  - [19] P.   hberg, *Phys. Rev. A* **59**, 634 (1999).
  - [20] K. L. Lee, N. B. Jorgensen, I-K. Liu, L. Wacker, J. J. Arlt, and N. Proukakis, *Phys. Rev. A* **94**, 013602 (2016).
  - [21] D. S. Petrov, *Phys. Rev. Lett.* **115**, 155302 (2015).
  - [22] V. Cikojevi  , K. D  zelalija, P. Stipanovi  , L. Vranje   Marki  , and J. Boronat, *Phys. Rev. B* **97**, 140502(R) (2018).
  - [23] C. R. Cabrera, L. Tanzi, J. Sanz, B. Naylor, P. Thomas, P. Cheiney, and L. Tarruell, *Science* **359**, 301 (2018).
  - [24] G. Semeghini, G. Ferioli, L. Masi, C. Mazzinghi, L. Wolswijk, F. Minardi, M. Modugno, G. Modugno, M. Inguscio, and M. Fattori, *Phys. Rev. Lett.* **120**, 235301 (2018).
  - [25] See for instance J. Boronat and J. Casulleras, *Phys. Rev. B* **49**, 8920 (1994).
  - [26] J. Casulleras and J. Boronat, *Phys. Rev. B* **52**, 3654 (1995).
  - [27] J. Pade, *Eur. Phys. J. D* **44**, 345 (2007).
  - [28] D. S. Petrov and G. E. Astrakharchik, *Phys. Rev. Lett.* **117**, 100401 (2016).
  - [29] D. Edler, C. Mishra, F. W  chtler, R. Nath, S. Sinha, and L. Santos, *Phys. Rev. Lett.* **119**, 050403 (2017).